Three-dimensional shape dependence of spin-wave modes in single FePt nanomagnets

R. Brandt,[1] F. Ganss,[2] R. Rückriem,[2] T. Senn,[3] C. Brombacher,[2] P. Krone,[2] M. Albrecht,[2] and H. Schmidt[1,*]

[1]*School of Engineering, University of California–Santa Cruz, Santa Cruz, California 95064, USA*

[2]*Institute of Physics, Chemnitz University of Technology, 09126 Chemnitz, Germany*

[3]*Institute of Nanometer Optics and Technology, Helmholtz Center Berlin for Materials and Energy, 12489 Berlin, Germany*

(Received 8 March 2012; revised manuscript received 22 August 2012; published 21 September 2012)

We report the dependence of the intrinsic spin-wave spectra on the three-dimensional shape in single FePt nanomagnetic elements. In contrast to the well-known center and edge modes in flat, circular nanodisks, curved nanomagnets with identical nominal thickness and footprint exhibit a rich multimode spectrum with qualitatively different dependence on applied field, such as a low-frequency "pinned" mode. Dynamic micromagnetic modeling shows that the experimentally observed modes originate from different sections of the nanomagnet with vastly different demagnetization fields. Thus, controlled shaping of a nanomagnet in all three dimensions creates the possibility of magnetization dynamics by design.

DOI: 10.1103/PhysRevB.86.094426 PACS number(s): 75.78.Jp, 75.50.Bb, 75.75.Jn

I. INTRODUCTION

Two-dimensional patterning of magnetic films and its effect on magnetization dynamics have been widely studied due to the relevance for a fundamental understanding of magnetism, as well as applications such as magnetic random access memory[1,2] and patterned magnetic data storage.[3,4] While spin dynamics in idealized geometries such as infinite films or ellipsoids of revolution can be treated analytically, the situation in realistic structures of finite size is more complex due to nonuniform internal fields within the element. A number of shapes, including ellipses, squares, wires, and asymmetric "eggs," have been studied,[5–15] with varying parameters such as size or aspect ratio,[7–9] as well as applied field direction.[10] One common observation is the formation of spin-wave wells, that is, regions that can support localized magnetization oscillations.[16] Systems that are symmetric with respect to the applied field direction produce symmetric center and edge mode distributions, while asymmetry results in a commensurate splitting of the oscillation modes, as the demagnetization field is no longer equal for opposite ends of the element.[11]

These studies have illustrated that controlling the shape of the magnetic element elicits a well-defined dynamic response. However, so far, structural control has been limited to two-dimensional patterning, that is, only controlling the footprint of an element while keeping a uniform profile in the vertical dimension. Recently, self-assembled nanospheres were used as a substrate to produce close-packed arrays of curved, magnetically isolated, single-domain nanomagnets.[17] These magnetic "caps" exhibit unique magnetostatic properties, including a change in easy axis direction and thickness due to the curvature of the spheres. Furthermore, their quasistatic switching characteristics deviate from simple Stoner–Wohlfarth behavior as a result of the relative geometry of the applied field angle and the varying easy axis direction across the cap.

In this paper, we report the magnetization dynamics of single nanomagnets with different three-dimensional shapes. Nanomagnets formed by the deposition of chemically disordered $Fe_{55}Pt_{45}$ films onto 100-nm-diameter SiO_2 spheres show vastly different spin-wave spectra compared to flat disks of the same thickness and diameter. The flat disks exhibit two main modes in which frequencies increase with applied field strength and where oscillations are concentrated in the center and edge regions. The spherically shaped caps, on the other hand, exhibit up to four oscillation modes with qualitatively different field dependencies. The large discrepancy in the magnetization dynamics results from the relative orientation of the applied field direction and the curvature of the magnetic element, which creates regions of varying demagnetizing field across the spherical cap.

II. EXPERIMENT

Close-packed arrays of SiO_2 nanospheres were created by the method proposed by Micheletto *et al.*[18] on thermally oxidized silicon substrates. This approach involves a self-assembly process, which is mainly driven by capillary forces in an aqueous colloid, where the water is evaporating under controlled conditions. A 20-nm-thick $Fe_{55}Pt_{45}$ film and 2-nm-thick Pt capping layer were deposited at room temperature on the nanosphere array by DC magnetron cosputtering from pure-element targets at an Ar pressure of 3.5×10^{-3} mbar. The iron content of 55 ± 1 at.% in the alloy was measured by Rutherford backscattering spectroscopy. A saturation magnetization of $\mu_0 M_S = 1.27$ T was determined by vibrating sample magnetometry. The film has a uniform thickness in the direction perpendicular to the substrate, but the curvature of the sphere's surface causes a radial change in the actual thickness from center to edge (Fig. 1(b) cartoon cross section). Measuring the intrinsic magnetization dynamics free from dipolar effects and nonmagnetic oscillation modes present in a close-packed array[19–21] requires use of single magnetic elements. To isolate a spherical cap, sample areas that were sparsely populated with spheres were identified. Then, focused ion-beam milling was used to remove the surrounding magnetic film to an outer diameter of 6–8 μm, which is larger than our probe spot size. As an example, Figure 1(b) shows a scanning electron microscope (SEM) image of an isolated nanosphere.

For preparation of the flat dot samples, a plane silicon substrate with an antireflective (AR) coating was spin-coated

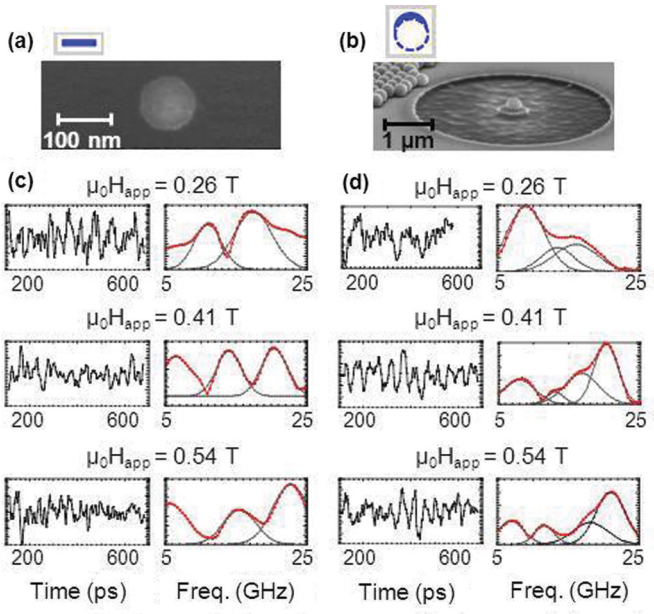

FIG. 1. (Color online) SEM images of (a) an individual flat nanodot and (b) a nanosphere after ion-beam milling isolation (cartoon cross sections shown above). Experimental TR-MOKE data for a $d = 100$ nm (c) flat disk and (d) spherical cap at three applied field strengths (listed above each trace). The left columns show the background-subtracted time traces, and the right columns display the corresponding FFT spectra with the Gaussian peak fits included (gray lines).

with Polymethyl methacrylate (PMMA) film and was patterned by electron beam lithography. After deposition of an identical layer stack as described above, the PMMA mask was removed by a wet chemical lift-off process. The AR-coated substrate (designed for a wavelength of 800 nm) improves the signal-to-noise ratio of magneto-optical measurements by reducing probe beam reflections from the area surrounding the investigated dots.[22]

The intrinsic spin-wave modes of single magnetic elements were measured using a previously described time-resolved magneto-optical Kerr effect microscope (TR-MOKE).[23] The ultrafast pulses from a Coherent Mira Ti:Sapphire laser are split into pump (wavelength = frequency-doubled 400 nm, $\sim$10.6 mW/μm^2) and probe (wavelength = 800 nm, $\sim$2.65 mW/μm^2) pulses. The heating of the relatively strong pump beam causes an ultrafast demagnetization followed by a small-angle precession around the effective field.[24,32] The probe beam travels through an optical delay line and linear polarizer before being focused to a spot size of $\sim$1 μm into the pumped area using a 60 $\times$ microscope objective (N.A. = 0.85). The change in polarization of the probe beam is measured using a crossed-polarizer configuration, and is recorded as a function of delay time between the pump and probe pulses. Another path analyzes the change in reflectivity (no polarizer before the detector), and is used to identify nonmagnetic signals present in the measurement. Small permanent magnets produce an externally applied field, the strength of which can be varied ($\mu_0 H_{app} = 0.25$ T to 0.55 T with an angle of 30° $\pm$ 2° from the sample plane). It is important to note that the nanomagnets are saturated for all applied field strengths, independent of shape, as verified by hysteresis loop measurements (not shown).

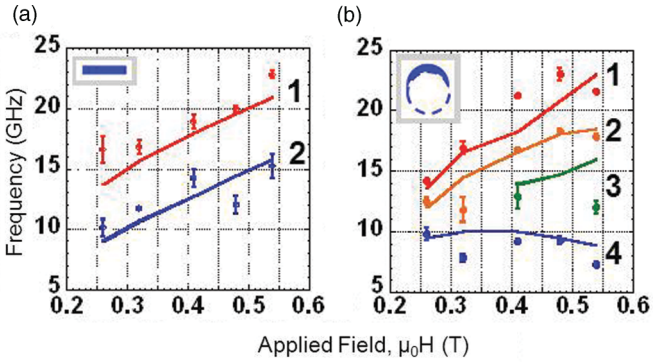

FIG. 2. (Color online) Peak frequencies as a function of applied field for a $d = 100$ nm (a) flat disk and (b) spherical cap. The symbols with error bars represent the experimental data, while the solid lines correspond to micromagnetic simulation.

To extract the magnetic oscillation frequencies from the time trace data, the thermally induced background is eliminated by subtracting a monoexponential decay from the raw Kerr signal. Then, a fast Fourier transform (FFT) is taken, and the spin-wave frequencies are identified by comparing the crossed-polarizer (magnetic) signal to the (nonmagnetic) reflectivity signal, which is representative of the noise spectrum in the measurement. Once the magnetic peaks are positively identified over several scans, we fit a sum of Gaussians to those peaks in the FFT trace. The error in fitting the peak position gives the value of the error bars for experimental data. Figure 1(c) and 1(d) shows example time trace data (left columns) and corresponding FFT spectra (right columns, individual Gaussian fits shown for identified spin-wave modes) for a spherical cap and flat disk of 100 nm diameter at three applied field strengths.

III. RESULTS AND DISCUSSION

The peak oscillation frequencies extracted for single 100-nm-diameter flat disks and spherical caps as a function of applied field are presented as symbols with error bars in Figure 2. It is clearly seen that the frequency spectra of the disk and cap differ considerably. The flat disk [Fig. 2(a)] shows two main modes that increase in frequency with applied field. For the spherical cap, however, there are up to four oscillation modes for a given field strength [Fig. 2(b)]. In addition to two modes that show an increase in resonance frequency with applied field (similar to the flat disk), the lowest-frequency modes remarkably show very little field dependence. This represents a clear, qualitative difference in the spin-wave spectra that is induced by the difference in three-dimensional shape.

In order to predict the oscillation frequencies and to better understand how the shape affects the dynamic response, micromagnetic simulations were performed using the Magpar[33] and FEMME[25] micromagnetic packages. The numerical simulations are based upon the Landau-Lifshitz-Gilbert (LLG) equation, which describes the motion of the

magnetization:

$$\frac{d\vec{M}}{dt} = -\gamma_0\mu_0\vec{M} \times \vec{H}_{\text{eff}} + \frac{\alpha}{M_S}\vec{M} \times \frac{d\vec{M}}{dt}, \qquad (1)$$

where γ_0 is the electron's gyromagnetic ratio, α is the Gilbert damping constant, M_S is the saturation magnetization, μ_0 is the permeability of free space, and $\boldsymbol{H}_{\text{eff}}$ is the effective field that represents various energy contributions in the system, such as shape anisotropy and the externally applied field. The simulations were run assuming no crystalline anisotropy, an exchange constant of 10^{-11} J/m, and using the measured M_S and H_{app}.

The simulated peak frequencies are plotted in Figure 2 as solid lines, and the agreement with the experimental data is rather good. The simulations reproduce the two measured frequency modes of the flat disk, and furthermore, the spherical cap simulations exhibit three modes for the lower field strengths ($\mu_0 H_{\text{app}} < 0.41$ T) and four at the higher field strengths ($\mu_0 H_{\text{app}} \geqslant 0.41$ T). Importantly, the existence of a qualitatively different, "pinned" low-frequency mode in the caps is also predicted.

In order to first develop a qualitative understanding for the complexity of the nanocap spin-wave spectra, we examine the demagnetizing field (H_d) present in the caps. Figure 3 shows the x-component of the simulated H_d for a slice taken through the middle of the spherical cap at an applied field of $\mu_0 H_{\text{app}} = 0.54$ T. The H_d distribution of the spherical cap shows several distinct regions: On the left side, which is aligned with the applied field, H_d is much smaller than on the right side, where the applied field is pushing the magnetization out of its easy axis direction. Based on the varying regions of H_d in the cap, the micromagnetic model of the cap can be divided into four sections, corresponding to the left edge, left center, right center, and right edge. Magpar allows for the simulated magnetic response to be averaged over each section (or for the entire structure). To simulate the small-angle precessions in Magpar, the magnetization was first relaxed in an external field with a slight offset of 0.1° in the y-direction with $\alpha = 1$. Then, the magnetization was relaxed in the external field with no offset, and the dynamics were recorded with $\alpha = 0.01$. The top row of Figure 3 shows the spin-wave spectrum of the entire cap, which exhibits four broad peaks. The sharpness of the individual modes is limited by the finite length of the simulation (~700 ps, in agreement with the experimental conditions). This indicates that the experimental data of Figure 1 are true representations of the spin-wave dynamics. The other frequency spectra show the localized oscillations in the four regions: The left edge and center are responsible for the highest-frequency mode, the right center contains signals from all three of the lower-frequency modes, and the right edge mainly exhibits one low-frequency oscillation. This relatively coarse segmentation of the cap shows that the distinct demagnetizing regions in the spherical cap, which arise due to the relative orientations of the three-dimensional curvature and applied field direction, are responsible for the observed complex multimode behavior.

However, to fully understand the mode spectrum of both curved and flat nanomagnets and obtain quantitative agreement

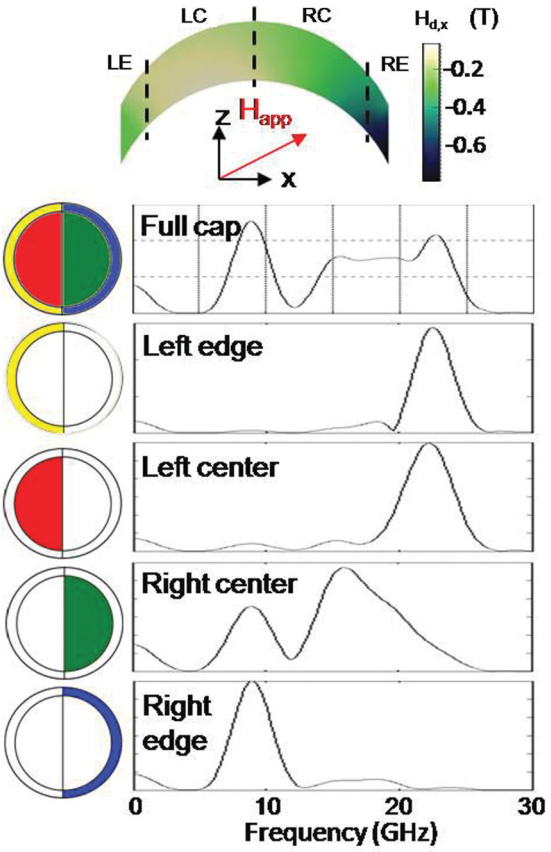

FIG. 3. (Color online) Simulated Fourier amplitude spectra of 100 nm spherical cap at an applied field of $\mu_0 H_{\text{app}} = 0.54$ T. The cross section of the cap shows the x component of the simulated demagnetizing field, with the applied field direction and color bar shown. The cap is broken up into four sections, and the frequency spectra show their respective oscillation frequencies.

with the experiment, more extensive micromagnetic analysis was performed, where each mesh node was analyzed to produce detailed spin-wave mode distributions using FEMME. After relaxation of the magnetization in a constant external field, a perpendicular pulse field of 1 mT with a duration of 100 ps was applied to excite magnetization oscillation in the linear regime for a simulation time of 4.0 ns and $\alpha = 0.01$. To visualize the spatial mode distribution, individual spin waves were excited with their respective precession frequency by an alternating field, which was applied perpendicular to the constant external field. By comparing minima and maxima of the z component (polar MOKE) of the magnetization of every finite-element mesh node (3.5 nm) during a simulation time of 10.0 ns (chosen to ensure at least 10 oscillations), an image of the oscillation amplitude distribution of each mode across the nanocap was produced.

Figure 4(a) and 4(c) shows the simulated x component of H_d for a flat dot and spherical cap ($\mu_0 H_{\text{app}} = 0.41$ T). Both side view and top view are pictured, and the applied field direction and scale bar are indicated in the middle. The H_d distribution for the flat dot shows distinct regions in the center and edge, which give rise to the well-known center and edge modes [Fig. 3(b)].[7] Specifically, the lower-frequency

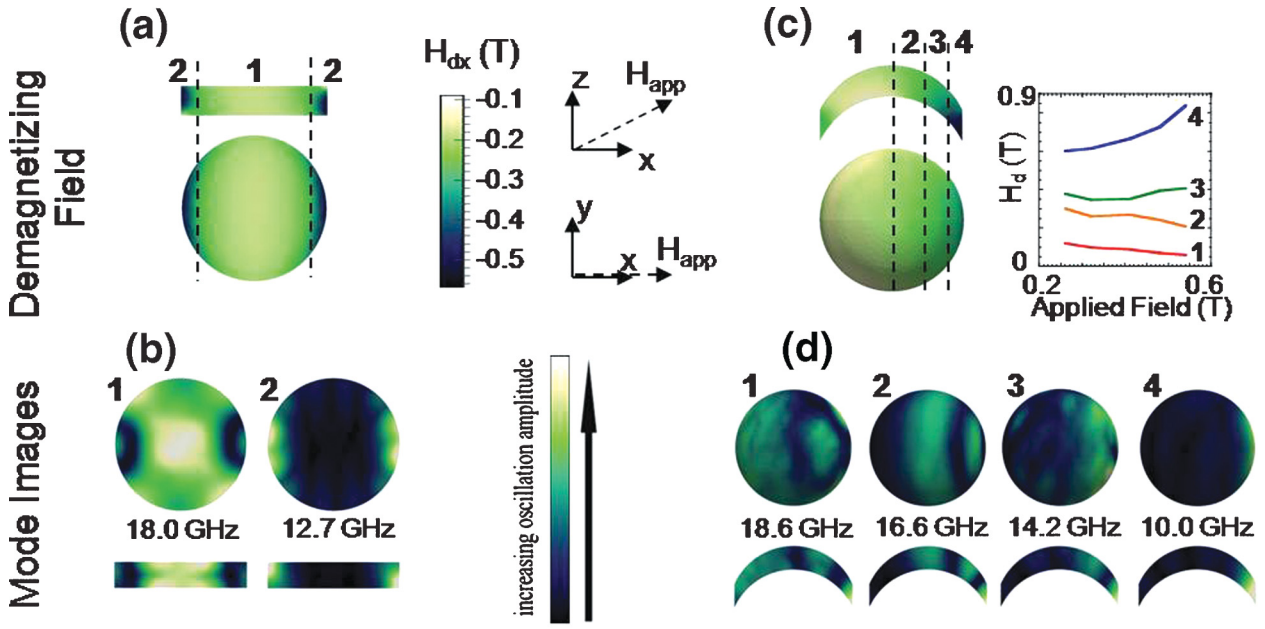

FIG. 4. (Color online) Demagnetizing field (a, c) and mode images (b, d) for a $d = 100$ nm (a, b) flat disk and (c, d) spherical cap ($\mu_0 H_{app} = 0.41$ T). The x component of H_d is shown for both side and top-down views with the applied field direction and color scale indicated in the center. The graph in (c) plots the average magnitude of H_d for the four spherical cap regions. The mode images in (b) and (d) (numbers correspond to the frequency branches in Fig. 2) are shown with the applied AC field frequencies listed, and are normalized from black (minimum oscillation amplitude) to white (maximum).

branch of the flat disk represents the edge mode, where a larger magnitude of H_d results in lower oscillation frequencies, since the overall effective field is reduced. As we saw in Figure 3, we expect the varying demagnetizing field in the sphere to produce several spatially confined modes. Indeed, the mode images for the spherical cap follow the demagnetizing regions quite closely [Fig. 4(d)]. It is seen that the left side produces one high-frequency mode, while the right side supports three separate modes that spatially correspond to the indicated regions in H_d. However, this more complete analysis reveals that the three high-frequency modes are somewhat delocalized across the sphere, while the fourth (low-frequency) mode is very strongly confined to the right side of the element.

All the simulated oscillation modes have similar field dependencies, except the edge mode on the far-right side of the spherical cap. In this case, the frequency varies very little as a function of applied field (lowest frequency, Fig. 2(b)). To explain this unusual field dependence, the graph in Fig. 4(c) shows the average magnitude of the demagnetizing field ($H_d = \sqrt{[H_{dx}{}^2 + H_{dy}{}^2 + H_{dz}{}^2]}$) of the four regions. The field dependence of each mode is a function of both H_{app} and H_d (resulting in H_{eff}), and, in general, H_d tends to reduce the overall H_{eff}. H_d is almost constant in regions 1–3; therefore, the field dependence tracks the slope of H_{app}. On the other hand, H_d in region 4 increases in magnitude with applied field and offsets the increase in frequency due to H_{app}, which results in the flat, "pinned" field dependence observed in the experiment. This steep increase in H_d is due to the relative geometry of the sphere and applied field (pushing the magnetization out of its easy axis) in combination with the tapering of the edge, which causes the magnetization to prefer the in-plane direction more strongly.

IV. SUMMARY

In summary, we have systematically investigated spin-wave spectra in single nanomagnetic caps, and we have described how their three-dimensional shape changes the frequency response as compared to flat dots of the same diameter and thickness. This can be attributed to the curvature of the spherical element and the applied field direction, which causes multiple distinct regions of demagnetizing field strength across the spherical cap. Deliberate three-dimensional shaping of a nanomagnetic element produces a richer interplay between the applied field direction and different segments of the magnetic element than conventional two-dimensional patterning. In particular, the appearance of new modes with qualitatively different dependencies on applied field provides additional opportunities for tailoring nanomagnet dynamics in the context of large-angle switching.[28–31]

ACKNOWLEDGMENTS

This work was supported by the National Science Foundation under Grants ECCS-0801896 and DMR-0806924, the Deutsche Forschungsgemeinschaft under Grant Al 618/5-1, the W. M. Keck Center for Nanoscale Optofluidics, and the International Research Training Group GRK 1215. The authors would like to thank M. Daniel for Rutherford backscattering spectroscopy measurements and analysis and Y. Yahagi for fruitful discussions and critical reading of this manuscript.

*Corresponding author: hschmidt@soe.ucsc.edu

[1] S. Kaka, M. R. Pufall, W. H. Rippard, T. J. Silva, S. E. Russek, J. A. Katine, and M. Carey, J. Magn. Magn. Mater. **286**, 375 (2005).
[2] R. C. Sousa and I. L. Prejbeanu, C. R. Phys. **6**, 1013 (2005).
[3] B. D. Terris and T. Thomson, J. Phys. D **38**, R199 (2005).
[4] T. Thomson, G. Hu, and B. D. Terris, Phys. Rev. Lett. **96**, 257204 (2006).
[5] J. P. Park, P. Eames, D. M. Engebretson, J. Berezovsky, and P. A. Crowell, Phys. Rev. Lett. **89**, 277201 (2002).
[6] G. Gubbiotti, M. Madami, S. Tacchi, G. Carlotti, A. O. Adeyeye, S. Goolaup, N. Singh, and A. N. Slavin, J. Magn. Magn. Mater. **316**, e338 (2007).
[7] V. V. Kruglyak, A. Barman, R. J. Hicken, J. R. Childress, and J. A. Katine, Phys. Rev. B **71**, 220409(R) (2005).
[8] A. Barman, S. Wang, J. D. Maas, A. R. Hawkins, S. Kwon, A. Liddle, J. Bokor, and H. Schmidt, Appl. Phys. Lett. **90**, 202405 (2007).
[9] P. S. Keatley, V. V. Kruglyak, A. Neudert, E. A. Galaktionov, R. J. Hicken, J. R. Childress, and J. A. Katine, Phys. Rev. B **78**, 214412 (2008).
[10] A. Barman, V. V. Kruglyak, R. J. Hicken, J. M. Rowe, A. Kundrotaite, J. Scott, and M. Rahman, Phys. Rev. B **69**, 174426 (2004).
[11] H. T. Nembach, J. M. Shaw, T. J. Silva, W. L. Johnson, S. A. Kim, R. D. McMichael, and P. Kabos, Phys. Rev. B **83**, 094427 (2011).
[12] J. M. Shaw, T. J. Silva, M. L. Schneider, and R. D. McMichael, Phys. Rev. B **79**, 184404 (2009).
[13] S. O. Demokritov, B. Hillebrands, and A. N. Slavin, IEEE Trans. Magn. **38**, 2502 (2002).
[14] V. V. Kruglyak, P. S. Keatley, R. J. Hicken, J. R. Childress, and J. A. Katine, Phys. Rev. B **75**, 024407 (2007).
[15] A. Neudert, P. S. Keatley, V. V. Kruglyak, J. McCord, and R. J. Hicken, IEEE Trans. Magn. **44**, 3083 (2008).
[16] J. Jorzick, S. O. Demokritov, B. Hillebrands, M. Bailleul, C. Fermon, K. Y. Guslienko, A. N. Slavin, D. V. Berkov, and N. L. Gorn, Phys. Rev. Lett. **88**, 047204 (2002).
[17] M. Albrecht, G. Hu, I. L. Guhr, T. C. Ulbrich, J. Boneberg, P. Leiderer, and G. Schatz, Nat. Mater. **4**, 203 (2005).
[18] R. Micheletto, H. Fukuda, and M. Ohtsu, Langmuir **11**, 3333 (1995).
[19] A. Barman and S. Barman, Phys. Rev. B **79**, 144415 (2009).
[20] R. F. C. Farrow, D. Weller, R. F. Marks, M. F. Toney, A. Cebollada, and G. R. Harp, J. Appl. Phys. **79**, 5967 (1996).
[21] A. Comin, C. Giannetti, G. Samoggia, P. Vavassori, D. Grando, P. Colombi, E. Bontempi, L. E. Depero, V. Metlushko, B. Ilic, and F. Parmigiani, Phys. Rev. Lett. **97**, 217201 (2006).
[22] N. Qureshi, S. Wang, M. A. Lowther, A. R. Hawkins, S. Kwon, A. Liddle, J. Bokor, and H. Schmidt, Nano Lett. **5**, 1413 (2005).
[23] A. Barman,S. Wang, O. Hellwig, A. Berger, E. E. Fullerton, and H. Schmidt, J. Appl. Phys. **101**, 09D102 (2007).
[24] M. van Kampen, C. Jozsa, J. T. Kohlhepp, P. LeClair, L. Lagae, W. J. M. de Jonge, and B. Koopmans, Phys. Rev. Lett. **88**, 227201 (2002).
[25] T. Schrefl, M. E. Schabes, D. Suess, O. Ertl, M. Kirschner, F. Dorfbauer, G. Hrkac, and J. Fidler, IEEE Trans. Magn. **41**, 3064 (2005).
[26] R. I. Joseph, J. Appl. Phys. **37**, 4639 (1966).
[27] C. Kittel, Phys. Rev. **73**, 155 (1948).
[28] C. Thirion, W. Wernsdorfer, and D. Mailly, Nat. Mater. **2**, 524 (2003).
[29] G. Woltersdorf and C. H. Back, Phys. Rev. Lett. **99**, 227207 (2007).
[30] H. W. Schumacher, C. Chappert, R. C. Sousa, P. P. Freitas, and J. Miltat, Phys. Rev. Lett. **90**, 017204 (2003).
[31] B. C. Choi, M. Belov, W. K. Hiebert, G. E. Ballentine, and M. R. Freeman, Phys. Rev. Lett. **86**, 728 (2001).
[32] B. Koopmans, in *Spin Dynamics in Confined Magnetic Structures II*, edited by B. Hillebrands and K. Ounadjela, Topics Appl. Phys. Vol. 87 (Springer-Verlag, Berlin, Heidelberg, 2003), pp. 253–323.
[33] W. Scholz, J. Fidler, T. Schrefl, D. Suess, R. Dittrich, H. Forster, and V. Tsiantos, Comput. Mater. Sci. **28**, 366 (2003).